# Density Functional Theory Study of H and CO Adsorption on Alkali-Promoted Mo2C Surfaces

**ARTICLE** *in* THE JOURNAL OF PHYSICAL CHEMISTRY C · MARCH 2011

Impact Factor: 4.77 · DOI: 10.1021/jp200950a



**3 AUTHORS**, INCLUDING:

Jeong Woo Han
University of Seoul
**37** PUBLICATIONS **399** CITATIONS

THE JOURNAL OF PHYSICAL CHEMISTRY C

ARTICLE

pubs.acs.org/JPCC

# Density Functional Theory Study of H and CO Adsorption on Alkali-Promoted $Mo_2C$ Surfaces

Jeong Woo Han, Liwei Li, and David S. Sholl*

School of Chemical and Biomolecular Engineering, Georgia Institute of Technology, 311 Ferst Drive, Atlanta, Georgia 30332-0100, United States

**ABSTRACT:** Using alkali metals as promoters is known to strongly influence the selectivity of catalytic reactions on $Mo_2C$ catalysts. To provide fundamental information about this observation, density functional theory calculations have been performed to study K and Rb adsorption of seven low-index α-$Mo_2C$ surfaces and the equilibrium crystal shape of $Mo_2C$ has been predicted using the Wulff construction. K and Rb are found to bind most strongly on $Mo_2C$ (001). This surface is also shown to favor a reconstruction in the absence of adsorbates. This reconstruction strengthens the adsorption of K and H while it weakens the adsorption of CO on the surface. A small number of calculations of H/K and CO/K coadsorption were performed to probe the effect of alkali promoters on these adsorbed species.

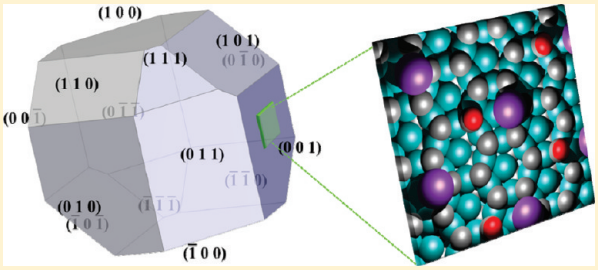


## 1. INTRODUCTION

Transition metal carbides are interesting as catalysts because of their extreme hardness,[1] high melting point,[2] and excellent electric and thermal conductivities.[3] Within this class of materials, molybdenum carbides have exhibited excellent catalytic behavior in reactions including ammonia synthesis,[4] water−gas shift,[5] hydrogenation of CO[6,7] or benzene,[8,9] hydrodenitrogenation,[10] hydrodesulfurization,[11] and hydrocarbon isomerization.[12] Molybdenum carbides are potentially promising substitutes for expensive noble metals due to their similar catalytic properties,[13] accompanied by resistance to sulfur poisoning.[13,14]

In the Mo−C phase diagram at least six different phases have been identified,[15] including two phases of $Mo_2C$ (one orthorhombic and one hexagonal). Among these phases, only two types of $Mo_2C$ and one MoC phase are found to be stable at room temperature.[15,16] There is some confusion in the literature regarding the names of $Mo_2C$ phases, with some authors referring to orthorhombic $Mo_2C$ as α-$Mo_2C$.[17−21] We prefer to follow the convention defined by the Joint Committee on Power Diffraction Standards (JCPDS) data files,[22−24] in which hexagonal $Mo_2C$, orthogonal $Mo_2C$, and hexagonal MoC are denoted α, $\beta$, and $\gamma$, respectively. $\beta$-$Mo_2C$ has been studied extensively since it has a well-determined structure in which carbon atoms occupy half of octahedral sites in an ordered way. In α-$Mo_2C$, Mo atoms form a hexagonally close packed structure while carbon atoms fill half of octahedral interstitial site randomly. In order to study the structure of α-$Mo_2C$, various carbon occupancy structures were proposed and investigated in literature,[25,26] and the eclipsed configuration identified by Haines et al.[26] was found to be most stable. We restrict our attention in this work to this eclipsed hexagonal configuration.

The surface properties of catalytic materials can be modified by doping with alkali metals.[27−33] Since K is relatively inexpensive, it is widely used as a promoter in industrial applications. Woo et al. reported significant changes in the selectivity to $C_1$−$C_7$ linear alcohols production relative to hydrocarbons from synthesis gas for experiments in which molybdenum carbides were promoted with $K_2CO_3$.[14] Xiang et al. have reported in experiments for mixed alcohol synthesis from CO hydrogenation that both $\beta$-$Mo_2C$ and α-$MoC_{1-x}$ produced light hydrocarbons and by adding K as a promoter, they showed a distinctive selectivity shift from hydrocarbons to alcohols.[29] In general terms, this promotion effect is thought to be associated with the charge transfer to the catalyst surface due to the exceptionally low ionization potential of alkali metals. The addition of alkali promoters generates electrostatic fields at the surface, inducing substantial changes in the process of adsorption and catalytic reactions.[32]

Theoretical studies have been applied to a range of physical, chemical, and electronic properties of the molybdenum carbides, including the adsorption and reaction of small species on the surfaces. Hugosson et al. have extensively examined the relative stabilities of Mo−C phases and the effect of vacancies on phase stability.[15] Kitchin et al. investigated the $\beta$-$Mo_2C$ (001) [$\beta$-$Mo_2C$ (0001) in their notation] surface along with the close-packed surfaces of other carbides to compare the chemical properties of various carbide surfaces.[34] DFT calculations for the adsorption of small molecules on $\beta$-$Mo_2C$ (001) have been also performed, including the adsorption $O_2$ and CO[35] [α-$Mo_2C$ (0001) in their notation], $CO_2$, H, $CH_x$ ($x$ = 0−3), $C_2H_4$[20,35] [α-$Mo_2C$ (0001) in their notation], and methanol.[36] Tominaga et al. have studied

**Received:** January 28, 2011
**Revised:** March 4, 2011
**Published:** March 21, 2011

individual reaction steps associated with several reactions on $\beta$-$Mo_2C$ (001) including the water-gas shift reaction,[37] $CH_4$ reforming,[38] and hydrodesulfurization of thiophene.[39] In all of these studies, it appears that attention was given to the (001) surface because this is most densely packed surface of $\beta$-$Mo_2C$. Shi et al. reported DFT calculations for a range of low-index surfaces of α-$Mo_2C$ [$\beta$-$Mo_2C$ in their notation][25] and further investigated CO and NO adsorption and dissociation on α-$Mo_2C$ (001).[40] They observed that the mixed Mo/C termination of the (011) surface, not (001), had the lowest surface free energy among the surfaces they considered. Pistonesi et al. recently studied the K promoter effect on dissociation of methanol on the $\beta$-$Mo_2C$ (001) surface.[41] None of the existing DFT studies of α-$Mo_2C$ have considered the properties of alkali atom as a promoter on the surface. A small number of DFT calculations are available examining this issue on other materials.[42,43]

In this paper, we use DFT calculations to probe the properties of alkali atoms on α-$Mo_2C$ surfaces with the aim of providing fundamental information about this situation that will be useful for considering the mechanistic influence of alkali promoters in complex catalytic reactions. To make progress toward this goal, we assume that the catalytic activity of $Mo_2C$ is associated with the terraces of stable surfaces of the material rather than being dominated by a rate-determining step dictated by a step edge or other defects. This assumption also underlies the DFT studies listed above, although it is rarely stated explicitly. This assumption means that we confine our attention to the properties of alkali adsorbed on stable surfaces on typical $Mo_2C$ crystals. We also consider situations where the concentration of alkali metal on catalyst particles is low. This choice implies that we must determine what $Mo_2C$ surfaces on a typical catalyst particle bind K most strongly. To this end, we examine the adsorption energies and geometries of K and Rb on seven low-index surfaces to determine the most preferred surface for their adsorption. An interesting finding from our calculations is that the bulk-terminated surface that binds K and Rb most strongly undergoes a surface reconstruction in the absence of any adsorbed species. The reconstructed surface binds K even more strongly than the bulk-terminated surface. We have examined the coadsorption of H or CO with K on this reconstructed surface to give some initial insight into the influence of K on reactant adsorption on this material. We note that the aim of this paper is not to provide a complete description of the effects of promoters on catalytic selectivity on $Mo_2C$. Rather, we lay the groundwork for tackling this challenging task in the future by systematically examining the properties of promoter species on a wide range of $Mo_2C$ surfaces.

## 2. COMPUTATIONAL DETAILS

Our plane wave DFT calculations were performed with the Vienna ab initio simulation package (VASP).[44−47] We employed the revised Perdew-Burke-Ernzerhof (rPBE) generalized gradient functional[48,49] along with the projector augmented wave (PAW)[50,51] method to describe ionic cores. A plane wave expansion with a cutoff of 400 eV was used for all calculations. Geometries were relaxed using a conjugate gradient algorithm until the forces on all unconstrained atoms were less than 0.03 eV/Å.

The α-$Mo_2C$ phase has an hexagonal crystal structure, with $a$ = 3.011 Å, $b$ = 3.011 Å, and $c$ = 4.771 Å.[52] The DFT-optimized hexagonal lattice constants for α-$Mo_2C$ phase ($a$ = 6.08 Å, $b$ = 6.07 Å, and $c$ = 4.72 Å) are in good agreement with the experimental values (here we have to double $a$ and $b$ because the original unit cell from experiment needs to be extended to define the eclipsed configuration unit cell). This bulk structure is illustrated in Figure 1. Calculations with the bulk structure confirmed that this material is metallic.

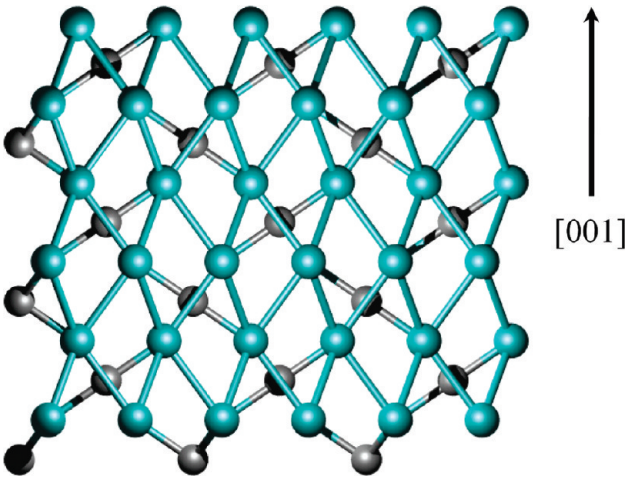


**Figure 1.** Most stable bulk structure of α-$Mo_2C$ phase viewed along the [010] axis. Mo (C) atoms are shown as green (gray) spheres.

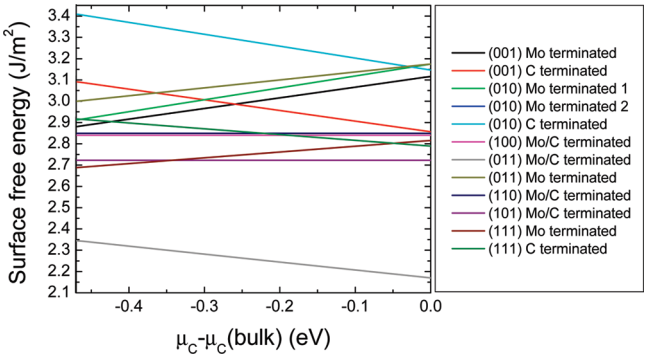


**Figure 2.** Surface free energies of seven low Miller index surfaces are plotted as a function of $\mu_c - \mu_c$(bulk). For each surface, the results for all possible terminations are shown.

We cleaved this structure along seven low Miller index planes, namely (001), (010), (100), (110), (101), (011), and (111), to construct surfaces. Each surface was represented by slabs 10−15 Å thick. All possible bulk terminations perpendicular to the surface normal to these planes were considered. The (001), (010), and (111) surfaces have both pure Mo and pure C terminations. The (100), (110), and (101) surfaces have mixed Mo/C terminations. The (011) surface has a pure Mo termination and a mixed Mo/C termination. In all calculations, no atoms in the slab were constrained and a vacuum spacing of 14 Å was used normal to the surface.

In all of our calculations the surfaces were constructed as symmetric slabs. This implies that some of the surface slabs were nonstoichiometric. As a result, the surface energy, $\sigma$, is calculated by[25,53−56]

$$\sigma = (E_{slab} - n_{Mo}\mu_{Mo} - n_C\mu_C)/2A \quad (1)$$

Here, $E_{slab}$ is the total energy of the slab, $A$ is the surface area of one side of the slab, $\mu_x$ is the chemical potential of species $x$, and $n_y$ is the number of atoms of species $y$ in the supercell. After some

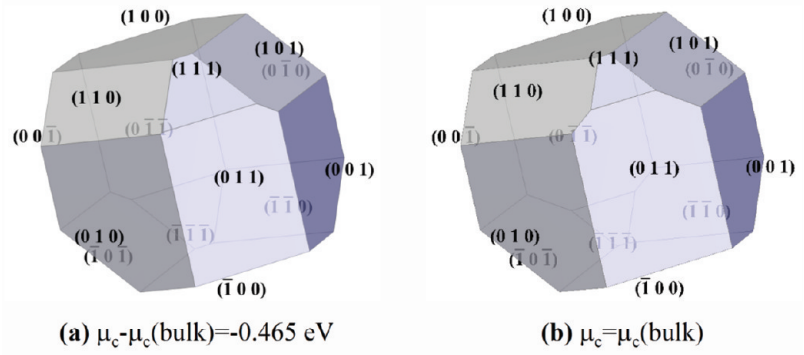


**Figure 3.** Predicted equilibrium crystal shapes of $Mo_2C$ determined from the Wulff construction using the surface free energies at the lower and upper bound of $\mu_c - \mu_c(\text{bulk})$.

algebra using the relationships described by previous reports,[25,53−56] the surface energy can be expressed as a function of difference between the chemical potential for a C atom, $\mu_C$, and the chemical potential in bulk phase of C, $\mu_C(\text{bulk})$. If a surface is stoichiometric within the symmetric slabs, eq 1 can be reduced to the usual expression for the surface energy[47]

$$\sigma = (E_{\text{slab}} - nE_{\text{bulk}})/2A \quad (2)$$

where $E_{\text{bulk}}$ is the bulk total energy per $Mo_2C$ unit and $n$ is the number of $Mo_2C$ units in the slab. In earlier work, Shi et al. compared the surface energies of different terminations using eq 2, and then used the predictions from these calculations to compare the surface energies of a variety of low-index surfaces.[25] This approach is potentially problematic because differing surface terminations should be compared using eq 1. In our work, we calculated the surface energy for each surface with each possible terminations using eq 1, as shown in Figure 2. In Figure 2, the C-terminated (010) surface has the highest surface free energy at almost all the ranges of $\mu_c - \mu_c(\text{bulk})$. Details regarding the definition and interpretation of $\mu_c - \mu_c(\text{bulk})$ are given in the earlier work by Shi et al.[25] The lowest surface free energy is found for the mixed Mo/C-terminated (011) surface, in agreement with Shi et al.'s calculations.

Calculations for adsorbed K on each surface were performed at various coverages to understand coverage effects as discussed later. A $6 \times 6 \times 1$ Monkhorst-Pack $k$-point mesh was used for a $(1 \times 1)$ surface unit cell, which was sufficient to give well converged results. For calculations at lower coverages, the number of $k$-points in the Monkhorst-Pack meshes was appropriately reduced. Calculations for H and CO adsorption with or without coadsorbed K were performed using a $(2 \times 2)$ surface unit cell with a $3 \times 3 \times 1$ Monkhorst-Pack $k$-point mesh. Geometries and energies for gas phase species were calculated using supercells equivalent to those for the largest slab calculations. When examining adsorption, molecules were placed on only one side of the slab. Dipole corrections were therefore applied in computing all of the energies reported below.[57,58] The adsorption energy, $E_{\text{ads}}$, of an atom or molecule was defined by

$$E_{\text{ads}} = (E_{\text{surf}} + E_{\text{adsorbate}}) - E_{\text{total}} \quad (3)$$

where $E_{\text{total}}$ is the total energy of the system containing the adsorbed species, $E_{\text{surf}}$ is the total energy for the optimized bare surface, and $E_{\text{adsorbate}}$ is the total energy for the adsorbate in the gas phase. With this definition, positive adsorption energies correspond to energetically favored states.

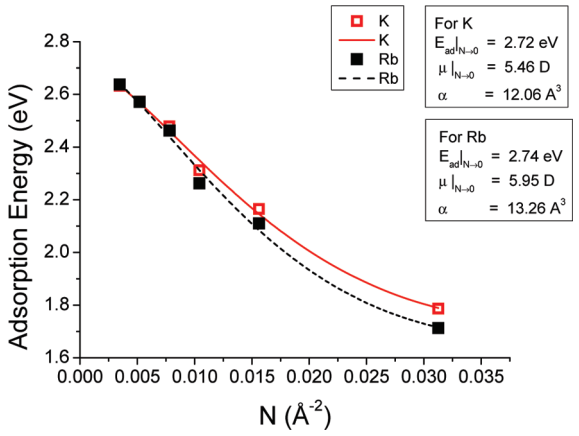


**Figure 4.** Adsorption energy of K and Rb as a function of coverage on $Mo_2C(001)$. The solid curve shows a fit of the data to the Albano model.[70]

## 3. RESULTS AND DISCUSSION

As can be seen from Figure 2, the range of surface energies among the set of surfaces we examined is not large, with energies varying from 2.2 to 3.4 J/m$^2$. Once the surface energies are known, the equilibrium crystal shape (ECS) of the material can be predicted from the Wulff construction.[59−62] We used this approach to examine the ECS for a range of carbon chemical potentials. Figure 3 shows the resulting ECS at the upper and lower bounds for $\mu_C$. Intermediate values of the $\mu_C$ give similar results. One immediate observation from this figure is that the (001) surface, which has been the focus of much earlier theoretical work, is not the only dominant surface on $Mo_2C$ crystals in terms of the surface area associated with this surface.

**3.1. K Adsorption on α-$Mo_2C$ Surfaces.** As described in section 1, we are interested in determining the location of adsorbed K in the limit of low K coverages on a catalyst particle. We have therefore examined K adsorption on the seven low Miller index surfaces mentioned in section 2. For these calculations only the termination with the lowest surface energy among the terminations we examined on each surface was considered except for the (001) surface, for which we considered both Mo-term and C-term since they had similar surface free energy.

Figure 4 shows an example of the calculated K adsorption energy at six surface coverages on α-$Mo_2C(001)$. Coverage is expressed in terms of the absorbate number density in Å$^{-2}$. In order to have confidence that a global minimum can be identified,

**Table 1. Adsorption Energies and Dipole Moments of K in the Limit of Zero Coverage for the Seven Surfaces Obtained As Described in the Text**

| surface | C-term (001) | Mo-term (001) | (100) | (110) | (010) | (011) | (101) | (111) |
|---|---|---|---|---|---|---|---|---|
| $E_{ad}\|_{N\to 0}$(eV) | 2.72 | 2.00 | 2.21 | 1.84 | 1.70 | 2.31 | 1.96 | 2.70 |
| $\mu\|_{N\to 0}$(D) | 5.46 | 3.41 | 3.83 | 3.29 | 1.95 | 4.41 | 2.95 | 4.26 |

large numbers of adsorption configurations must be examined for studying atomic or molecular adsorption.[63−66] To address this challenge, we examined a variety of initial configurations by dividing a $(1 \times 1)$ surface unit cell of the (001) surface into a $4 \times 3$ grid at intervals of ~1.6 Å. K is then positioned 3.3 Å above each grid point so that we have 12 initial configurations for adsorption on the surface. Each configuration was relaxed to find a local energy minimum for the adsorbed molecule. The structure with the most stable adsorption energy among the energy minima found in this way was used to perform lower coverage calculations. The adsorption energies shown in Figure 4 are the results of these coverage dependent calculations.

Figure 4 shows that the adsorption energy of K is strongly dependent upon coverage. This is not surprising, as strong repulsive interactions induced by the dipole moment of adsorbed K are expected. Based on the steep work function changes upon the K adsorption, Bugyi et al. suggested that the K promoter donates charge to the surface upon adsorption on this kind of surface.[30,31] Our charge calculations by Bader analysis[67−69] at the highest coverage, 32.0 Å$^2$/atom, support the observation, showing that a charge of −0.9e is transferred into the surface from K. This charge transfer creates a dipole moment associated with an adsorbed K.

We can model the coverage dependent adsorption using a simple electrostatic method developed by Albano.[70] The coverage dependent adsorption energy is assumed to be entirely due to repulsive dipole−dipole interactions on the surface. This model has been successfully applied to several experiments including desorption of K from metal surfaces,[70] desorption of K in the presence of coadsorbed O,[70] molecular desorption of $CH_3Cl$ from Pd(100),[71] and atomic I desorption from Ni surfaces.[72] The Albano model can be written as

$$E_{ad} = E_{ad}|_{N\to 0} - 1.602 \times \frac{9 \times (\mu|_{N\to 0})^2 N^{3/2}}{(1 + 9\alpha N^{3/2})^2} \quad (4)$$

Here $E_{ad}$ is the adsorption energy (in eV), $E_{ad}|_{N\to 0}$ is the adsorption energy in the limit of zero coverage (in eV), $\mu|_{N\to 0}$ is the static dipole moment of the K−$Mo_2C$ surface bond in the limit of zero coverage (in Debye), N is the surface coverage in atoms (in Å$^{-2}$), α is the constant polarizability of the adsorbed K (in Å$^3$), 9 is the geometric factor applicable to a hexagonal or square array of adsorbates, and 1.602 is the unit conversion factor. Fitting eq 4 to the data in Figure 4 gives $E_{ad}|_{N\to 0}$, $\mu|_{N\to 0}$, and α values of 2.72 eV, 5.46 D, and 12.06 Å$^3$, respectively.

We used an approach similar to the one described above to calculate the coverage dependent adsorption energies of K for the other surfaces. For simplicity, we assumed that the polarizability of adsorbed K is independent of the surface orientation and equal to the value deduced above, 12.06 Å$^3$. With this assumption the Albano model includes only two parameters, which we fitted for each surface from computed adsorption energies at three distinct coverages. Table 1 summarizes $E_{ad}|_{N\to 0}$ and $\mu|_{N\to 0}$ for each surface. Among the seven surfaces, (001) has the highest adsorption energy and dipole moment. On this basis, we selected the (001) surface for further calculations involving coadsorption of H or CO with K.

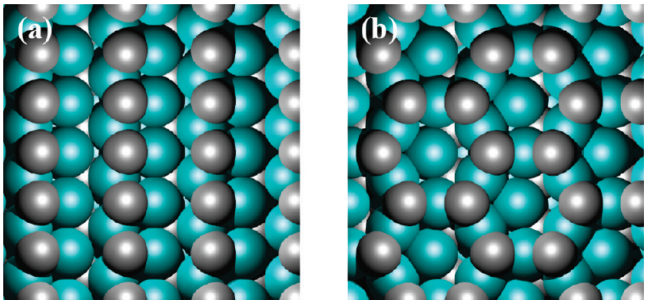


**Figure 5.** (a) Unreconstructed and (b) reconstructed bare (001) surface. Mo atoms are shown as green spheres and C atoms as gray spheres.

**3.2. Rb Adsorption on α-$Mo_2C$ Surfaces.** To examine whether the results for K also apply to other alkali metals, we also studied Rb adsorption on $Mo_2C$ (001) surface as a comparison with K adsorption. Calculations were performed at the same set of coverages as for K, and the Albano model was again used to fit the data. The results are shown in Figure 4. The geometry, adsorption energy, and dipole moment (as determined from the Albano model) are very similar for Rb and K.

**3.3. K, H, and CO Adsorption on Bare Unreconstructed and Reconstructed α-$Mo_2C$ (001) Surfaces.** We noted above that most previous DFT calculations examining surfaces of α−$Mo_2C$ used the (001) surface, even though later calculations by Shi et al.[25] showed that the (011) surface has a markedly lower surface energy. Our analysis of K binding energies, however, suggests that it is quite appropriate to focus attention on the (001) surface if we are interested in low coverages of K on catalyst particles. While performing calculations with α-$Mo_2C$(001), however, we made the interesting observation that this surface can reconstruct, even in the absence of adsorbates. Figure 5 shows both unreconstructed and reconstructed bare (001) surfaces. The surface energy is lowered by 0.18 J/m$^2$ for any value of $\mu_c$-$\mu_c$(bulk) by this reconstruction. This structure was initially observed in calculations involving CO adsorption, but subsequent calculations confirmed that the reconstructed bare surface in the absence of CO has 1.47 eV/unit cell lower total energy than the unreconstructed one. During the reconstruction, C atoms move in a way that they form hexagons on the surface with adjacent C atoms separated ~3.5 Å. Our reconstructed surface is similar to a honeycomb $(\sqrt{3} \times \sqrt{3})$R30 °C-terminated structure on α-$Mo_2C$(001) previously reported by scanning tunneling microscopy (STM)[73,74] except that our structure is missing a C atom in the middle of each hexagon. This observation implies that earlier calculations[20,35−39] examining adsorption on α-$Mo_2C$(001) may not capture all features of these systems because they did not include the surface reconstruction. The existence of a reconstruction for the (001) surface prompted us to consider whether surface reconstructions might also exist for some of the

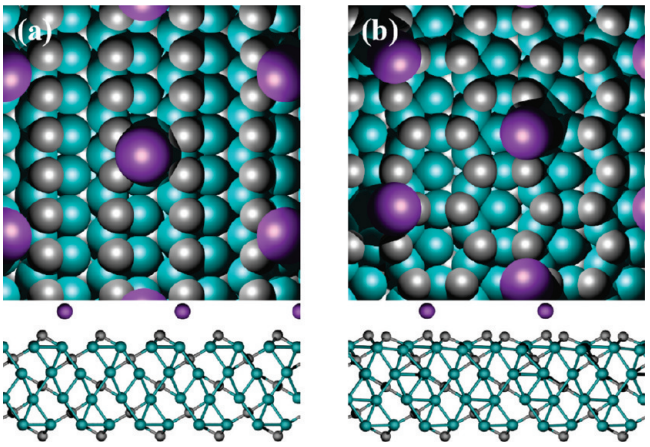


**Figure 6.** Top and side view of K adsorption on (a) unreconstructed and (b) reconstructed (001) surface. In addition to the atoms described in Figure 5, K atoms are shown in purple.

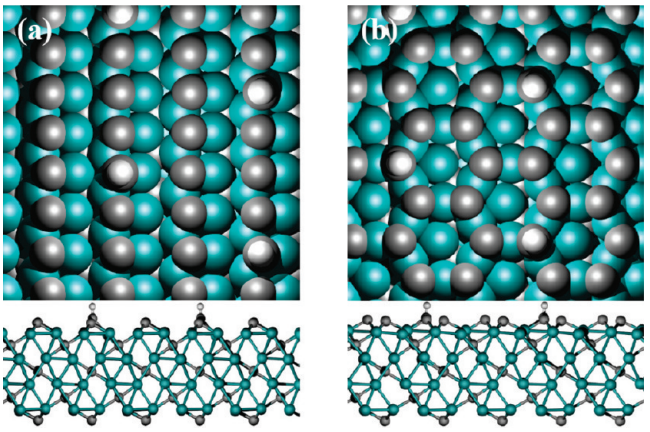


**Figure 7.** Top and side view of H adsorption on (a) unreconstructed and (b) reconstructed (001) surface. In addition to the atoms described in Figure 5, H atoms are shown in white.

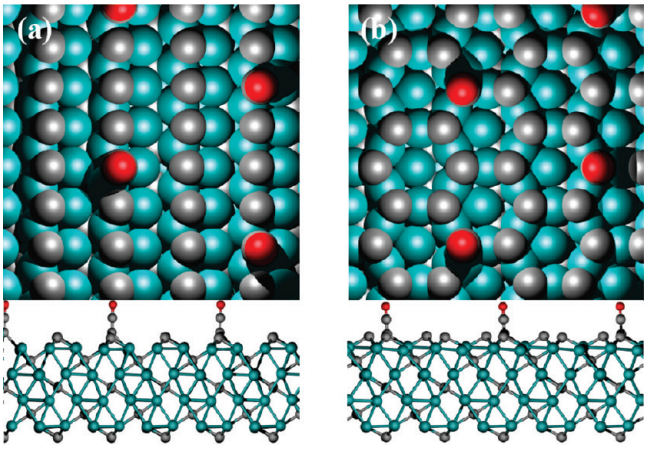


**Figure 8.** Top and side view of CO adsorption on (a) unreconstructed and (b) reconstructed (001) surface. In addition to the atoms described in Figure 5, O atoms are shown in red.

other surfaces we have considered. It is of course not possible to make any definitive statements about this possibility, but examination of the other surfaces shown in Figure 2 based on coordination-based arguments did not suggest any obvious candidates for reconstruction.

Above, we argued that adsorption of K on the unreconstructed (001) surface is the most stable among the surfaces we considered. It is therefore important to compare K adsorption on the bulk terminated and reconstructed (001) surfaces. Possible adsorption sites on the reconstructed surface were determined as described above at a coverage of 32.0 $Å^2$/atom. The binding energy of K was then calculated in the most stable site on each surface with one K adsorbed in a $(2 \times 2)$ surface unit cell, which gives an area of 127.9 $Å^2$/atom. The results from these calculations are shown in Figure 6. K binds on the unreconstructed (001) surface by coordinating with two C atoms and two Mo atoms. On the reconstructed surface, the adsorbed atom is coordinated with three C atoms and three Mo atoms. The adsorption energy of K on the unreconstructed (reconstructed) surface at this coverage is 2.48 eV (2.64 eV). That is, the reconstructed surface binds K more tightly than the unreconstructed surface and is therefore an appropriate surface to consider when examining the properties of K at low coverage on catalyst particles.

H adsorption on both the unreconstructed and reconstructed bare surfaces has also been examined. Initial configurations for both surfaces were constructed in the same way as for K adsorption. The adsorption coverage of H we present here is 127.9 $Å^2$/atom with one H adsorbed in a $(2 \times 2)$ surface unit cell. After all calculations, the most stable structures of H adsorption on both surfaces are found as shown in Figure 7. H adsorption on each surface is preferred on the atop site of a C atom. For both cases, the bond length between C and H atoms is 1.10 Å, which is a typical C−H bond length. The adsorption energy of H on the reconstructed surface (1.02 eV) is 0.35 eV larger than on the unreconstructed surface (0.67 eV), indicating that this surface reconstruction would be strongly favored by the presence of adsorbed H. This adsorption energy for H is given relative to half of total energy of $H_2$ molecule in the gas phase.

We also examined CO adsorption on the same surfaces. The same coverage as in the K or H adsorption was used for CO adsorption. Initial configurations were constructed in a same way as in the adsorption of K or H for both surfaces. It is known that CO vertically adsorbs onto this kind of surface where the C atom contacts the surface,[35,75] so we primarily considered this case. To verify this approach, however, adsorption states with the O atom toward the surface and various CO bond tilt angles were also examined. The CO adsorption structures in the most stable states for both surfaces are shown in Figure 8. The structure with the O atom closer to the surface showed almost zero adsorption energy and all the tilt angle cases were found to converge to C-down-O-up configuration. As shown in Figure 8, the CO adsorption on an atop site of C atom is energetically most favorable for each surface. We calculated the vibrational frequency of CO adsorption on the reconstructed $Mo_2C$ (001) surface within the harmonic approximation. The CO stretch frequency from our calculation was 2066 $cm^{-1}$, which is consistent with a recent in situ IR spectra study of CO adsorbed on fresh $\beta$-$Mo_2C$ that observed a CO vibrational peak between 2054−2071 $cm^{-1}$.[75] Ren et al. also demonstrated from their GGA-PBE DFT calculations that CO adsorption on the atop site C atom forming C═C═O is energetically favored among CO adsorption states on C-terminated $\beta$-$Mo_2C$ (001).[35] We calculated the adsorption energy of CO on the unreconstructed (reconstructed) surface to be 1.65 eV (1.51 eV). For this case, the adsorption on the reconstructed

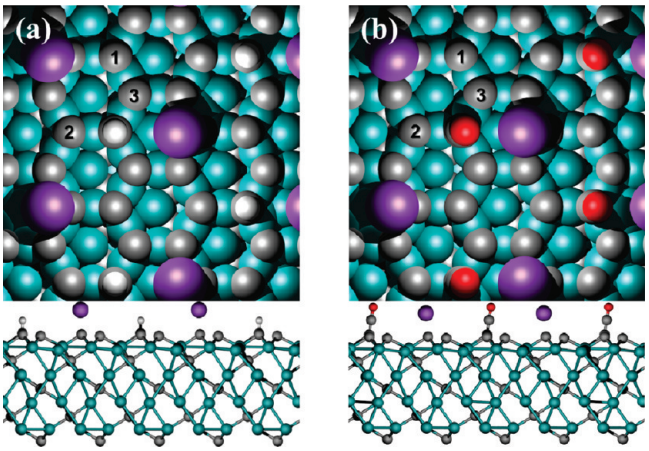


**Figure 9.** Top and side view of (a) H coadsorption and (b) CO coadsorption with K promoter on reconstructed (001) surface. Less stable adsorption sites for H or CO with K are also marked as 1−3.

**Table 2. Adsorption Energies in the Most Stable and Less Stable Configurations for H and CO Coadsorbed with K**

| $E_{ad}$ (eV) | most stable | 1 | 2 | 3 |
|---|---|---|---|---|
| H/K | 0.88 | 0.84 | 0.69 | 0.67 |
| CO/K | 1.44 | 1.39 | 1.40 | 1.41 |

surface is less energetically favored to on the unreconstructed one. This energy difference however, is not sufficient to reverse the overall stability of the surface reconstruction at the CO coverages we examined.

**3.4. H or CO coadsorption with K promoter on reconstructed α−$Mo_2C$ (001) surfaces.** Finally, we examined H/K and CO/K coadsorption on α−$Mo_2C$ (001). Initial configurations were constructed with linear combinations of K and H or CO adsorbed structures in their most stable states. The most stable configurations for H and CO coadsorbed with K are shown in Figure 9. Their most stable adsorption structures are very similar in local geometry to the situation when the species are separately adsorbed. The less stable adsorption sites and their adsorption energy are also shown in Figure 9 and Table 2. For H adsorption, we also considered configurations that involved formation of KH, since K is known to form a stable bulk hydride.[76] These calculations indicated that formation of surface KH is not favored relative to the adsorption of H directly on the surface. The adsorption energy of H referenced to the energy of the optimized K adsorbed structure is 0.88 eV, which is 0.14 eV less than the adsorption energy of H on the nonpromoted surface. For CO/K coadsorption, the bond length between a C atom in the molecule and C atom on each surface is same as in adsorption of CO without K. The adsorption energy of CO referenced to the energy of the optimized K adsorbed structure is 1.44 eV, which is reduced by 0.07 eV from CO adsorption on the bare surface. The reduction in adsorption energy for CO and H in the presence of adsorbed K is reasonable since the dipole moment of adsorbed CO or H will have the same orientation as the dipole moment of adsorbed K, leading to a repulsive adsorbate−adsorbate interaction. This initial examination of coadsorption with K atoms is not sufficient to draw conclusions about the overall effect of K on catalytic reactivity on this surface, but it should provide useful baseline data for future investigations of these issues.

## 4. CONCLUSION

In order to provide fundamental information on how the adsorption of alkali metals can affect $Mo_2C$ catalysts, DFT calculations were performed to study the stability of seven low-index bare surfaces of α-$Mo_2C$ and the adsorption of K on those surfaces. We used the Wulff construction to predict the equilibrium crystal shape of $Mo_2C$ using surface energies calculated from DFT. Even though (011) surface has the lowest surface energy, we found that at low coverages, K atoms adsorb more strongly on the (001) surface. The adsorption of Rb was found to be very similar to the adsorption of K.

During further investigation of the (001) surface, we observed a surface reconstruction that is favored for the bare surface in which the top layer of C atoms on the surface form hexagonal arrays. The adsorption of K and H was energetically favored on the reconstructed (001) surface, although CO was observed to bind more favorably to the unreconstructed surface. Preliminary calculations of H or CO coadsorption with K on the (001) surface showed that each species remains to its most stable site on the bare surface, although the adsorption energy of H and CO is reduced upon coadsorption with K. Our results do not make direct predictions about the role of K promoters in the catalytic selectivity of α-$Mo_2C$ surfaces, but by providing the first precise information about how K atoms bind on these surfaces they provide a useful foundation for future examinations of the interesting issue of catalytic selectivity. Our calculations were based on the presence of K on the surface as an atomic species. It is conceivable that under catalytic reaction conditions, other species involving K can also exist. Our calculations examined this possibility for KH, finding that this hydride species is quite unstable relative to coadsorption of K and H. Our calculations did not probe, however, other possible K-containing surface species such as hydroxides or carbonates, so determining the stability of these kinds of species may be useful in the future.

## AUTHOR INFORMATION

**Corresponding Author**
*E-mail: david.sholl@chbe.gatech.edu.

## ACKNOWLEDGMENT

Financial support from the Dow Chemical Company is gratefully appreciated, as are fruitful discussions with Prof. Christopher Jones, Prof. Pradeep Agrawal (Georgia Tech), and Prof. Robert Davis (University of Virginia).

## REFERENCES

(1) Liao, J. J.; Wilcox, R. C.; Zee, R. H. *Scripta. Metall. Mater.* **1990**, *24*, 1647.
(2) Hwu, H. H.; Chen, J. G. *Chem. Rev.* **2005**, *105*, 185.
(3) Nelson, J. A.; Wagner, M. J. *Chem. Mater.* **2002**, *14*, 4460.
(4) Kojima, R.; Aika, K. *Appl. Catal. A-Gen.* **2001**, *219*, 141.
(5) Patt, J.; Moon, D. J.; Phillips, C.; Thompson, L. *Catal. Lett.* **2000**, *65*, 193.
(6) Ranhotra, G. S.; Bell, A. T.; Reimer, J. A. *J. Catal.* **1987**, *108*, 40.
(7) Park, K. Y.; Seo, W. K.; Lee, J. S. *Catal. Lett.* **1991**, *11*, 349.
(8) Lee, J. S.; Yeom, M. H.; Lee, D. S. *J. Mol. Catal.* **1990**, *62*, L45.

(9) Lee, J. S.; Yeom, M. H.; Park, K. Y.; Nam, I. S.; Chung, J. S.; Kim, Y. G.; Moon, S. H. *J. Catal.* **1991**, *128*, 126.
(10) Schwartz, V.; da Silva, V. T.; Oyama, S. T. *J. Mol. Catal. A-Chem.* **2000**, *163*, 251.
(11) Rodriguez, J. A.; Dvorak, J.; Jirsak, T. *Surf. Sci.* **2000**, *457*, L413.
(12) Ledoux, M. J.; Cuong, P. H.; Guille, J.; Dunlop, H. *J. Catal.* **1992**, *134*, 383.
(13) Oyama, S. T. *Catal. Today* **1992**, *15*, 179.
(14) Woo, H. C.; Park, K. Y.; Kim, Y. G.; Nam, I. S.; Chung, J. S.; Lee, J. S. *Appl. Catal.* **1991**, *75*, 267.
(15) Hugosson, H. W.; Eriksson, O.; Nordstrom, L.; Jansson, U.; Fast, L.; Delin, A.; Wills, J. M.; Johansson, B. *J. Appl. Phys.* **1999**, *86*, 3758.
(16) Velikanova, T. Y.; Kublii, V. Z.; Khaenko, B. V. *Sov. Powder. Metall. Met. Ceram.* **1988**, *27*, 891.
(17) Liu, P.; Rodriguez, J. A.; Hou, H.; Muckerman, J. T. *J. Chem. Phys.* **2003**, *118*, 7737.
(18) Liu, P.; Rodriguez, J. A. *J. Chem. Phys.* **2004**, *120*, 5414.
(19) Liu, P.; Rodriguez, J. A.; Asakura, T.; Gomes, J.; Nakamura, K. *J. Phys. Chem. B* **2005**, *109*, 4575.
(20) Ren, J.; Huo, C. F.; Wang, J. G.; Cao, Z.; Li, Y. W.; Jiao, H. J. *Surf. Sci.* **2006**, *600*, 2329.
(21) Ren, J.; Wang, J. G.; Huo, C. F.; Wen, X. D.; Cao, Z.; Yuan, S. P.; Li, Y. W.; Jiao, H. J. *Surf. Sci.* **2007**, *601*, 1599.
(22) *Powder Diffraction File*; JCPDS International Center for Diffraction Data: Pennsylvania, 2004.
(23) Piquemal, J.-Y.; Potvin, C.; Manoli, J.-M.; Djéga-Mariadassou, G. *Catal. Lett.* **2004**, *92*, 189.
(24) Pielaszek, J.; Mierzwa, B.; Medjahdi, G.; Mareche, J. F.; Puricelli, S.; Celzard, A.; Furdin, G. *Appl. Catal. A-Gen.* **2005**, *296*, 232.
(25) Shi, X. R.; Wang, S. G.; Wang, H.; Deng, C. M.; Qin, Z. F.; Wang, J. G. *Surf. Sci.* **2009**, *603*, 852.
(26) Haines, J.; Leger, J. M.; Chateau, C.; Lowther, J. E. *J. Phys.-Condens. Mat.* **2001**, *13*, 2447.
(27) Kotarba, A.; Adamski, G.; Piskorz, W.; Sojka, Z.; Sayag, C.; Djega-Mariadassou, G. *J. Phys. Chem. B* **2004**, *108*, 2885.
(28) Xiang, M. L.; Li, D. B.; Xiao, H. C.; Zhang, J. L.; Li, W. H.; Zhong, B.; Sun, Y. H. *Catal. Today* **2008**, *131*, 489.
(29) Xiang, M. L.; Li, D. B.; Li, W. H.; Zhong, B.; Sun, Y. H. *Fuel* **2006**, *85*, 2662.
(30) Bugyi, L.; Oszko, A.; Solymosi, F. *Surf. Sci.* **2000**, *461*, 177.
(31) Bugyi, L.; Solymosi, F. *J. Phys. Chem. B* **2001**, *105*, 4337.
(32) King, D. A.; Woodruff, D. P. *The Chemical Physics of Solid Surfaces, Coadsorption, Promoters and Poisons*; Elsevier: Amsterdam, 1993; Vol. 6.
(33) Haider, M. A.; Gogate, M. R.; Davis, R. J. *J. Catal.* **2009**, *261*, 9.
(34) Kitchin, J. R.; Norskov, J. K.; Barteau, M. A.; Chen, J. G. *Catal. Today* **2005**, *105*, 66.
(35) Ren, J.; Huo, C. F.; Wang, J. G.; Li, Y. W.; Jiao, H. J. *Surf. Sci.* **2005**, *596*, 212.
(36) Pistonesi, C.; Juan, A.; Farkas, A. P.; Solymosi, F. *Surf. Sci.* **2008**, *602*, 2206.
(37) Tominaga, H.; Nagai, M. *J. Phys. Chem. B* **2005**, *109*, 20415.
(38) Tominaga, H.; Nagai, M. *Appl. Catal. A-Gen.* **2007**, *328*, 35.
(39) Tominaga, H.; Nagai, M. *Appl. Catal. A-Gen.* **2008**, *343*, 95.
(40) Shi, X.-R.; Wang, J.; Hermann, K. *J. Phys. Chem. C* **2010**, *114*, 13630.
(41) Pistonesi, C.; Juan, A.; Farkas, A. P.; Solymosi, F. *Surf. Sci.* **2010**, *604*, 914.
(42) Linic, S.; Barteau, M. A. *J. Am. Chem. Soc.* **2004**, *126*, 8086.
(43) Liu, Z.-P.; Hu, P. *J. Am. Chem. Soc.* **2001**, *123*, 12596.
(44) Kresse, G.; Furthmuller, J. *Phys. Rev. B* **1996**, *54*, 11169.
(45) Kresse, G.; Hafner, J. *Phys. Rev. B* **1993**, *47*, 558.
(46) Kresse, G.; Hafner, J. *J. Phys.: Condens. Matter* **1994**, *6*, 8245.
(47) Sholl, D. S.; Steckel, J. A. *Density functional theory: a practical introduction*; John Wiley & Sons, Inc.: Hoboken, NJ, 2009.
(48) Perdew, J. P.; Burke, K.; Ernzerhof, M. *Phys. Rev. Lett.* **1996**, *77*, 3865.
(49) Perdew, J. P.; Burke, K.; Ernzerhof, M. *Phys. Rev. Lett.* **1997**, *78*, 1396.
(50) Blöchl, P. E. *Phys. Rev. B* **1994**, *50*, 17953.
(51) Kresse, G.; Joubert, D. *Phys. Rev. B* **1999**, *59*, 1758.
(52) Rudy, E.; Windisch, S.; Stosick, A. J.; Hoffman, J. R. *Trans. Metall. So. Aime* **1967**, *239*, 1247.
(53) Siegel, D. J.; Hector, L. G.; Adams, J. B. *Surf. Sci.* **2002**, *498*, 321.
(54) Rapcewicz, K.; Chen, B.; Yakobson, B.; Bernholc, J. *Phys. Rev. B* **1998**, *57*, 7281.
(55) Batyrev, I.; Alavi, A.; Finnis, M. W. *Faraday Discuss.* **1999**, *114*, 33.
(56) Zhang, W.; Smith, J. R. *Phys. Rev. B* **2000**, *61*, 16883.
(57) Bengtsson, L. *Phys. Rev. B* **1999**, *59*, 12301.
(58) Neugebauer, J.; Scheffler, M. *Phys. Rev. B* **1992**, *46*, 16067.
(59) Wulff, G. *Z. Kryst. Mineral.* **1901**, *34*, 449.
(60) Shi, H. Q.; Stampfl, C. *Phys. Rev. B* **2008**, *77*, 094127.
(61) Soon, A.; Wong, L.; Delley, B.; Stampfl, C. *Phys. Rev. B* **2008**, *77*, 125423.
(62) Kim, K. C.; Dai, B.; Johnson, J. K.; Sholl, D. S. *Nanotechnology* **2009**, *20*, 204001.
(63) Šljivancanin, Ž.; Gothelf, K. V.; Hammer, B. *J. Am. Chem. Soc.* **2002**, *124*, 14789.
(64) Bhatia, B.; Sholl, D. S. *Angew. Chem., Int. Ed.* **2005**, *44*, 7761.
(65) Han, J. W.; Sholl, D. S. *Langmuir* **2009**, *25*, 10737.
(66) Han, J. W.; Sholl, D. S. *Phys. Chem. Chem. Phys.* **2010**, *12*, 8024.
(67) Henkelman, G.; Arnaldsson, A.; Jonsson, H. *Comput. Mater. Sci.* **2006**, *36*, 354.
(68) Sanville, E.; Kenny, S. D.; Smith, R.; Henkelman, G. *J. Comput. Chem.* **2007**, *28*, 899.
(69) Tang, W.; Sanville, E.; Henkelman, G. *J. Phys.-Condens. Mat.* **2009**, *21*, 084204.
(70) Albano, E. V. *J. Chem. Phys.* **1986**, *85*, 1044.
(71) Berko, A.; Erley, W.; Sander, D. *J. Chem. Phys.* **1990**, *93*, 8300.
(72) Myli, K. B.; Grassian, V. H. *Langmuir* **1995**, *11*, 849.
(73) Lo, R. L.; Fukui, K.; Otani, S.; Iwasawa, Y. *Surf. Sci.* **1999**, *440*, L857.
(74) Lo, R. L.; Fukui, K.; Otani, S.; Oyama, S. T.; Iwasawa, Y. *Jpn. J. Appl. Phys. 1* **1999**, *38*, 3813.
(75) Wu, W. C.; Wu, Z. L.; Liang, C. H.; Chen, X. W.; Ying, P. L.; Li, C. *J. Phys. Chem. B* **2003**, *107*, 7088.
(76) Kim, K. C.; Sholl, D. S. *J. Phys. Chem. C* **2010**, *114*, 678.